Chapter 12

Electromechanical Control over Effective Permittivity Used for Microwave Devices

Yuriy Prokopenko, Yuriy Poplavko, Victor Kazmirenko and Irina Golubeva

Additional information is available at the end of the chapter

http://dx.doi.org/10.5772/50584

1. Introduction

Ferroelectrics are well known tunable dielectric materials. Permittivity of these materials can be controlled by an applied electrical bias field. Controllable permittivity leads to alteration of characteristics of tunable microwave components such as propagation constants, resonant frequency etc. However, dielectric losses in the ferroelectric-type tunable components are comparatively high and show substantial increase approaching to the millimetre waves due to fundamental physical reason.

Alternative way to achieve controllability of characteristics in tunable microwave devices is mechanical reconfiguration. In this case the alteration of microwave characteristics can be attained by displacement of dielectric or metallic parts of devices. Mechanical tuning is very promising to produce low insertion loss combined with good tunability in microwave subsystems. In the case of ferroelectric technique of tuning, microwaves interact with the ferroelectric material which is a part of microwave line. That is why transmitted energy is partially absorbed by this material. On the contrary, mechanical system of control is located out of microwave propagation route so it does not contribute to the microwave loss. Moreover, it will be shown that dielectric losses have a trend to reduce in such devices. Mechanical control is valid at any frequency range, including millimetre wave range.

Transformation of microwave characteristics could be described in terms of medium's effective dielectric permittivity (ε_{eff}). Effective dielectric permittivity of inhomogeneous medium can be defined as dielectric permittivity of homogeneous medium, which brings numerically the same macro parameters to the system of the same geometrical configuration. Effective permittivity is convenient parameter to describe devices with TEM wave propagating, where propagation constant is proportional to $\sqrt{\varepsilon_{eff}}$, however it can be used to describe other devices as well.

Application of piezoelectric or electrostrictive actuators opens an opportunity for electromechanical control over effective dielectric permittivity in microwave devices [1]. However for such applications a tuning system should be highly sensitive to rather small displacement of device components. The key idea how to achieve such a high sensitivity of system characteristics to small displacement of device's parts is to provide a strong perturbation of the electromagnetic field in the domain influenced directly by the mechanical control. For that, a tunable dielectric discontinuity (the air gap) should be created perpendicularly to the pathway of the electric field lines. This air gap is placed between the dielectric parts or the dielectric plate and an electrode. An alteration of the air gap dimension leads to essential transformation in the electromagnetic field, and revising of components' characteristics such as resonant frequency, propagated wave phase, and so on.

The goal of this chapter is to describe electromagnetic field phenomena in structures suitable for electromechanical control of effective dielectric permittivity.

2. Dispersion properties of one-dimensional dielectric discontinuity

Simplest structure suitable for electromechanical alteration of microwave characteristics is presented in Figure 1. In this structure two dielectrics are placed between infinite metal plates. The thickness d of the dielectric in the domain 2 may be variable.

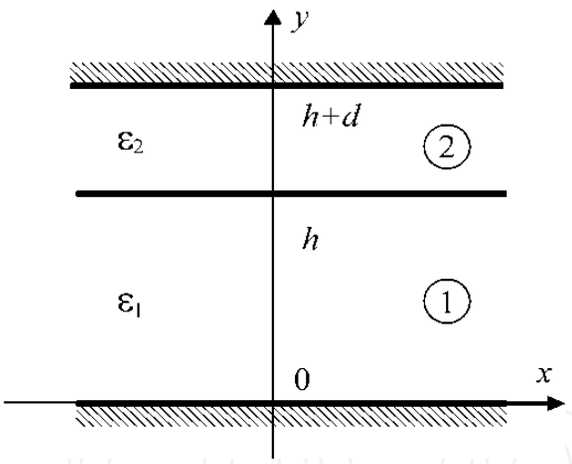

Figure 1. One-dimensional dielectric discontinuity

Electromagnetic field of this structure can be described in terms of LM and LE modes. Transverse wavenumber of the LM mode can be found from dispersion equations:

$$\begin{aligned} &\frac{\beta_{y1}^{e}}{\varepsilon_1}\tan\left(\beta_{y1}^{e}h\right)+\frac{\beta_{y2}^{e}}{\varepsilon_2}\tan\left(\beta_{y2}^{e}d\right)=0; \\ &\left(\varepsilon_1-\varepsilon_2\right)k^2=\beta_{y1}^{e\ 2}-\beta_{y2}^{e\ 2}, \end{aligned} \tag{1}$$

where $\beta_{y1(2)}^{e}$ is the transverse wavenumber in the region 1 or 2 respectively, $\varepsilon_{1(2)}$ is the permittivity of the region 1 or 2 respectively, h and d are thicknesses of regions 1 and 2

respectively, $k = \frac{\omega}{c}$ is the wavenumber in free space, ω is the circular frequency, c is the light velocity in vacuum.

Using equations (1) calculations of the transverse wavenumbers are carried out in a wide range of the permittivities and thicknesses of dielectrics in domains 1 and 2. It is found that the transverse wavenumbers as the solutions of equations (1) depend on frequency, permittivities of dielectrics and sizes of domains 1 and 2. Computed results are shown in Figure 2. This figure illustrates a dependence of normalized transverse wavenumber of domain 1 for fundamental LM mode versus the normalized air gap while permittivity of domains 2 is $\varepsilon_2 = 1$.

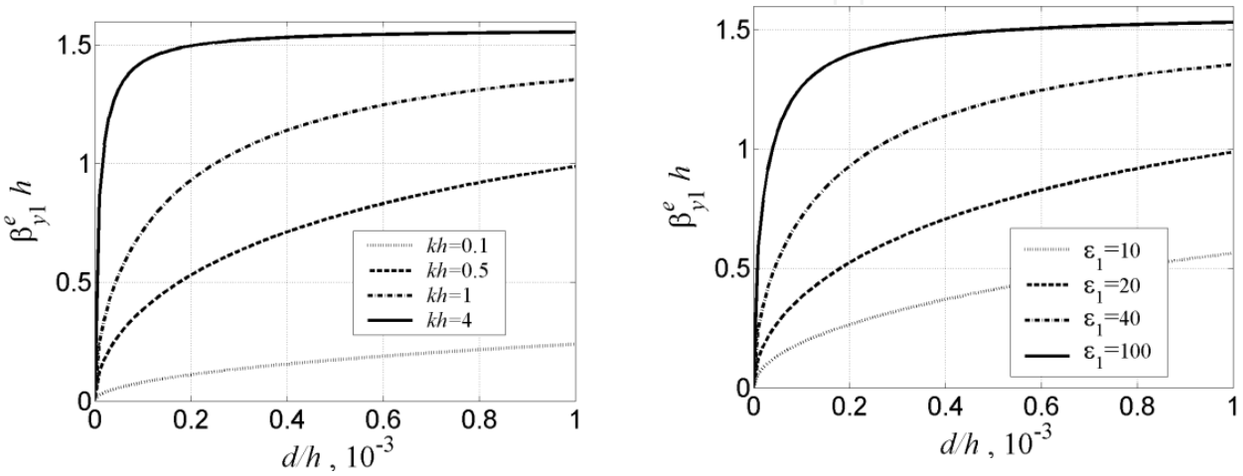

Figure 2. Normalized transverse wavenumber of fundamental LM mode versus normalized air gap size: (*a*) for certain normalized wavenumbers *kh* while ε1 = 80; (*b*) for various permittivities of dielectric in domain 1 while normalized wavenumber is *kh* = 2.

As it is seen, transverse wavenumber of LM mode is very sensitive to variation of air gap between dielectric and metal plate. The change in only tenth or even hundredth part of percent from size of dielectric in domain 1 is sufficient for considerable alteration of transverse wavenumber. Required absolute change of air gap for significant alteration is not more than tens or hundreds micrometres depending on wavelength band and permittivity of dielectric in domain 1.

In contrast to LM mode distribution of electromagnetic field of LE mode is significantly less sensitive to variation of air gap. Transverse wavenumbers β_{y1}^m and β_{y2}^m of the LE mode are solutions of the dispersion equations:

$$\begin{aligned} &\beta_{y1}^m \cot\left(\beta_{y1}^m h\right) + \beta_{y2}^m \cot\left(\beta_{y2}^m d\right) = 0; \\ &\left(\varepsilon_1 - \varepsilon_2\right) k^2 = {\beta_{y1}^m}^2 - {\beta_{y2}^m}^2. \end{aligned} \tag{2}$$

Figure 3 illustrates a dependence of transverse wavenumber β_{y1}^m of the basic LE mode on normalized air gap thickness. As it is seen, for the LE mode required change of air gap is

comparable with size of dielectric in domain 1 and quantitatively the alteration is appreciably less than for the LM mode.

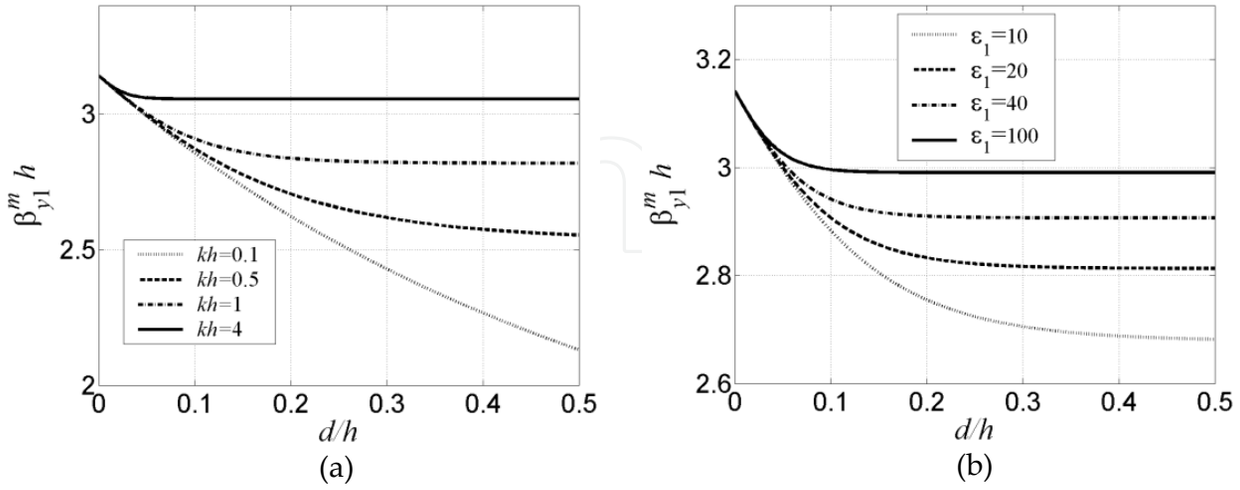

Figure 3. Normalized transverse wavenumber of basic LE mode versus normalized air gap size: (*a*) for certain normalized wavenumbers *kh* while $\varepsilon_1 = 80$; (*b*) for various permittivities of dielectric in domain 1 while normalized wavenumber is $kh = 2$.

Peculiarity of the LM mode is existence of E_y -component of electrical field which is directed normally to the border of dielectric discontinuity. For the LE mode the component E_y is equal to zero. Therefore to achieve considerable alteration of electromagnetic field a border should be located between dielectric and air to perturb normal component of the electric field. This principle should be applied to all of electromechanically controlled microwave devices.

If the domain 1 contains lossy dielectric characterized by the loss tangent tanδ, then transverse wavenumber is a complex value and its imaginary part defines dielectric loss. Figure 4 demonstrates dependences of imaginary part of normalized transverse wavenumber of domain 1 for fundamental LM mode versus the normalized air gap.

Negative values of the imaginary part say, that dielectric losses in the structure would be reduced in comparison with homogeneous structure. Moreover, for certain frequency and air gap size the dielectric loss reaches a minimum. This effect is fundamental and is observed in more complicated tunable structures.

Rigorous simulation of electromechanically controllable microwave devices requires solving of scattering problem on dielectric wedge placed between metal plates, Figure 5. Solution of the problem by the boundary element method (BEM) is discussed below.

3. Scattering on dielectric wedge placed between metal plates

Let's consider an incident wave impinging from domain 1 loaded by dielectric with permittivity ε_3 upon dielectric discontinuity in domain 2, Figure 5. Electromagnetic field of

this structure can be described in terms of LM and LE modes represented by y-component of electrical Γ^e and magnetic Γ^m Hertz vectors.

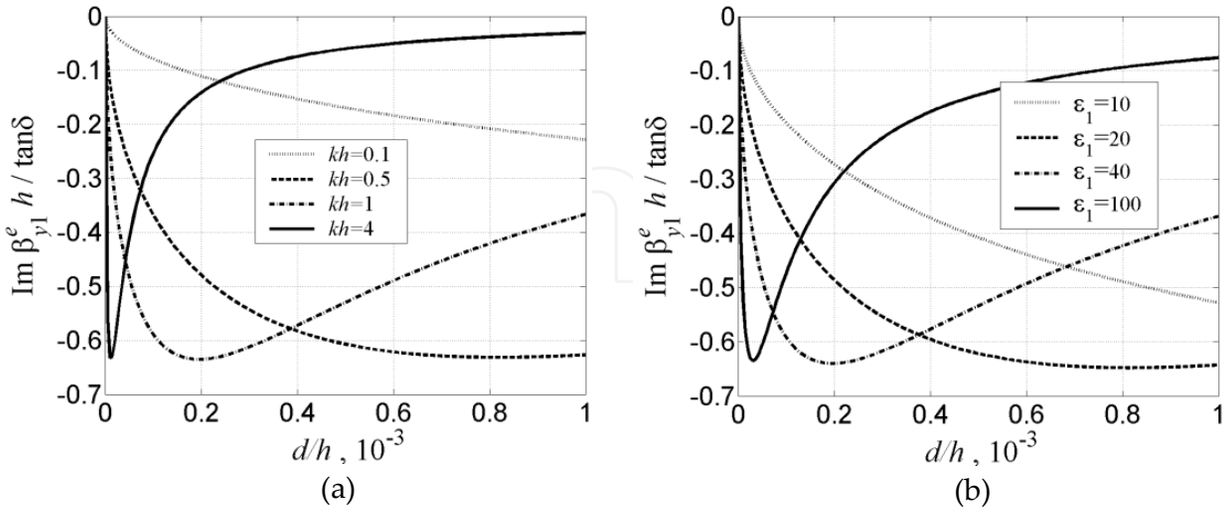

Figure 4. Imaginary part of normalized transverse wavenumber of fundamental LM mode versus normalized air gap size: (*a*) for certain normalized wavenumbers *kh* while ε1=80; (*b*) for various permittivities of dielectric in domain 1 while normalized wavenumber is *kh* = 2.

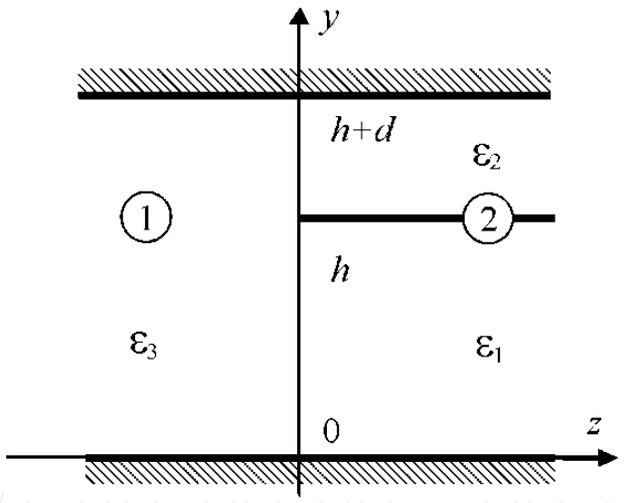

Figure 5. Structure that illustrated scattering problem

An incident wave in domain 1 is described by a sum of partial waves of LM and LE types:

$$\Gamma^{e+} = \sum_{i=0}^{n_e} c_i^e Y_{1i}^e(y) X^e(x) e^{-j\beta_{z_i} z},$$
$$\Gamma^{m+} = \sum_{i=1}^{n_m} c_i^m Y_{1i}^m(y) X^m(x) e^{-j\beta_{z_i} z}, \tag{3}$$

where $c_i^{e(m)}$ are amplitudes of partial waves, $Y_{1i}^e(y)$ and $Y_{1i}^m(y)$ are eigen functions of the domain 1, $X^e(x)$ and $X^m(x)$ are solutions of the Helmholtz equation

$\frac{d^2X^{e(m)}(x)}{dx^2}+\beta_x^2X^{e(m)}(x)=0$, β_x is a constant, $\beta_{zi}=\sqrt{\varepsilon_3k^2-\beta_{y1i}^2-\beta_x^2}$ is the propagation constant in domain 1, $\beta_{y1i}=\frac{i\pi}{h+d}$ is an eigen value of the domain 1, n_e is the quantity of incident LM modes, n_m is the quantity of incident LE modes. Eigen functions of the domain 1 are equal to

$$Y_{1i}^e(y)=\begin{cases}\sqrt{\frac{1}{h+d}}, & i=0\\ \sqrt{\frac{2}{h+d}}\cos(\beta_{y1i}y), & i\neq 0\end{cases}, \tag{4}$$

$$Y_{1i}^m(y)=\sqrt{\frac{2}{h+d}}\sin(\beta_{y1i}y). \tag{5}$$

Reflected wave is represented as series of the 1st domain's eigen functions as

$$\begin{aligned}\Gamma^{e-}&=\sum_{i=0}^{\infty}a_{1i}^eY_{1i}^e(y)X^e(x)e^{j\beta_{zi}z},\\ \Gamma^{m-}&=\sum_{i=1}^{\infty}a_{1i}^mY_{1i}^m(y)X^m(x)e^{j\beta_{zi}z},\end{aligned} \tag{6}$$

where $a_{1i}^{e(m)}$ are amplitudes of eigen modes.

Total electromagnetic field in the 1st domain is expressed as a composition of incident (3) and reflected (6) waves.

Electromagnetic field in the 2nd domain is represented as series of domain's eigen functions as

$$\begin{aligned}\Gamma_2^e&=\sum_{i=0}^{\infty}a_{2i}^e\rho(y)Y_{2i}^e(y)X_i^e(x)e^{-j\beta_{zi}^ez},\\ \Gamma_2^m&=\sum_{k=0}^{\infty}a_{2i}^mY_{2i}^m(y)X_i^m(x)e^{-j\beta_{zi}^mz},\end{aligned} \tag{7}$$

where $a_{2i}^{e(m)}$ are amplitude of eigen modes in the domain 2, $\rho(y)=\begin{cases}\sqrt{\varepsilon_1}, & y\le h\\ \sqrt{\varepsilon_2}, & h\le y\le h+d\end{cases}$ is the weight function, $\beta_{zi}^{e(m)}=\sqrt{\varepsilon_1k^2-\beta_{y1i}^{e(m)^2}-\beta_x^2}=\sqrt{\varepsilon_2k^2-\beta_{y2i}^{e(m)^2}-\beta_i^2}$ is the propagation constant of the domain 2, k is the propagation constant in free space, $\beta_{y1(2)i}^e$ are i-th solutions of the equations (1), $\beta_{y1(2)i}^m$ are eigen values of magnetic Hertz vector in the domain 2 computed from the equations (2), $Y_{2k}^{e(m)}(y)$ are eigen functions of the 2nd domain.

Eigen functions of the domain 2 are equal to

$$Y_{2i}^{e}(y)=\begin{cases}\dfrac{\cos\left(\beta_{y1i}^{e}y\right)}{N_i^{e}\varepsilon_1\cos\left(\beta_{y1i}^{e}h\right)}, & 0\le y\le h\\ \dfrac{\cos\left(\beta_{y2i}^{e}\left(y-h-d\right)\right)}{N_i^{e}\varepsilon_2\cos\left(\beta_{y2i}^{e}d\right)}, & h\le y\le h+d\end{cases}, \tag{8}$$

$$Y_{2i}^{m}(y)=\begin{cases}\dfrac{\sin\left(\beta_{y1i}^{m}y\right)}{N_i^{m}\sin\left(\beta_{y1i}^{m}h\right)}, & 0\le y\le h\\ \dfrac{\sin\left(\beta_{y2i}^{m}\left(h+d-y\right)\right)}{N_i^{m}\sin\left(\beta_{y2i}^{m}d\right)}, & h\le y\le h+d\end{cases}, \tag{9}$$

where $N_i^{e}=\sqrt{\dfrac{h}{2}+\dfrac{\sin\left(2\beta_{y1i}^{e}h\right)}{4\beta_{y1i}^{e}}+\dfrac{d}{2}+\dfrac{\sin\left(2\beta_{y2i}^{e}d\right)}{4\beta_{y2i}^{e}}}{\varepsilon_1\cos^2\left(\beta_{y1i}^{e}h\right)}+\dfrac{}{\varepsilon_2\cos^2\left(\beta_{y2i}^{e}d\right)}}$, $N_i^{m}=\sqrt{\dfrac{h}{2}-\dfrac{\sin\left(2\beta_{y1i}^{m}h\right)}{4\beta_{y1i}^{m}}+\dfrac{d}{2}-\dfrac{\sin\left(2\beta_{y2i}^{m}d\right)}{4\beta_{y2i}^{m}}}{\sin^2\left(\beta_{y1i}^{m}h\right)}+\dfrac{}{\sin^2\left(\beta_{y2i}^{m}d\right)}}$.

Using orthogonality property of eigen functions, amplitudes of eigen functions were expressed via indeterminate functions which are proportional to tangential components of electrical and magnetic field at the boundary of spatial domains:

$$f^{e}(y)=\frac{E_y}{X^{e}(x)}=\frac{\dfrac{\partial^2\Gamma_i^{e}}{\partial y^2}+\varepsilon_i(y)k^2}{X^{e}(x)},$$
$$f^{m}(y)=\frac{Z_0H_y}{X^{m}(x)}=Z_0\frac{\dfrac{\partial^2\Gamma_i^{m}}{\partial y^2}+\varepsilon_i(y)k^2}{X^{m}(x)}, \tag{10}$$

where i=1,2, $\varepsilon_i(y)=\begin{cases}\varepsilon_3, & i=1\\ \varepsilon_1, & 0\le y\le h\\ \varepsilon_2, & h\le y\le h+d\end{cases}, i=2$, $Z_0=\sqrt{\dfrac{\varepsilon_0}{\mu_0}}$ is the characteristic impedance of free space.

Equality requirement for another tangential components of electromagnetic filed reduces the scattering problem to set of Fredholm integral equations of the first kind for functions $f^{e}(y)$ and $f^{m}(y)$:

$$\int_0^{h+d}\left(G_j^{e}(y,y')f^{e}(y)+G_j^{m}(y,y')f^{m}(y)\right)dy=\phi_j(y),\quad j=1,2, \tag{11}$$

where kernels of integral equations $G_j^e(y,y')$ and $G_j^m(y,y')$ are expressed via eigen functions of domains 1 and 2:

$$G_1^e(y,y') = \pm\beta_x \sum_{i=0}^{\infty} \left(\frac{Y_{1i}^e(y') \frac{dY_{1i}^e(y)}{dy}}{\varepsilon_3 k^2 - \beta_{y1i}^2} - \frac{\rho^2(y') Y_{2i}^e(y') \frac{dY_{2i}^e(y)}{dy}}{\left(\varepsilon_1 k^2 - \beta_{y1i}^{e\ 2}\right)} \right), \tag{12}$$

$$G_1^m(y,y') = -k \sum_{i=0}^{\infty} \left(\frac{\beta_{zi} Y_{1i+1}^m(y') Y_{1i+1}^m(y)}{\varepsilon_3 k^2 - \beta_{y1i+1}^2} + \frac{\beta_{zi}^m Y_{2i}^m(y') Y_{2i}^m(y)}{\varepsilon_1 k^2 - \beta_{y1i}^{m\ 2}} \right), \tag{13}$$

$$G_2^e(y,y') = \omega\varepsilon_0 \sum_{i=0}^{\infty} \left(\frac{\varepsilon_3 \beta_{zi} Y_{1i}^e(y') Y_{1i}^e(y)}{\varepsilon_3 k^2 - \beta_{y1i}^2} + \frac{\varepsilon_2(y) \rho^2(y') \beta_{zi}^e Y_{2i}^e(y') Y_{2i}^e(y)}{\varepsilon_1 k^2 - \beta_{y1i}^{e\ 2}} \right), \tag{14}$$

$$G_2^m(y,y') = \mp \frac{\beta_x}{Z_0} \sum_{i=0}^{\infty} \left(\frac{Y_{1i+1}^m(y') \frac{dY_{1i+1}^m(y)}{dy}}{\varepsilon_3 k^2 - \beta_{y1i+1}^2} - \frac{Y_{2i}^m(y') \frac{dY_{2i}^m(y)}{dy}}{\varepsilon_1 k^2 - \beta_{y1i}^{m\ 2}} \right), \tag{15}$$

where ω is the circular frequency, ε_0 is the dielectric constant in vacuum, μ_0 is the magnetic constant. Sign in (12) depends on relation between signs in $\frac{dX^e(x)}{dx}$ and $X^m(x)$. If $\frac{dX^e(x)}{dx} = \beta_x X^m(x)$ then the sign "+" shall be applied in (12). However if $\frac{dX^e(x)}{dx} = -\beta_x X^m(x)$ then the sign of (12) shall be "—".

Functions $\phi_j(y)$ are described by incident partial waves:

$$\phi_1(y) = -2\omega\mu_0 \sum_{i=1}^{n_{1m}} \beta_{zi} c_{1i}^m Y_{1i}^m(y), \tag{16}$$

$$\phi_2(y) = 2\omega\varepsilon_0\varepsilon_3 \sum_{i=0}^{n_{1e}} \beta_{zi} c_{1i}^e Y_{1i}^e(y). \tag{17}$$

The set of integral equations (11) was solved by Galerkin method. Functions $f^e(y)$ and $f^m(y)$ were expanded in respect to basis $\varphi_0^{e(m)}(y)$, $\varphi_1^{e(m)}(y)$, … and set of integral

equations was reduced to a system of linear algebraic equations by ordinary Galerkin procedure.

For small values of *d*/*h* eigen functions of domains 1 and 2 were selected as a basis of the Galerkin method. However, for large values of *d*/*h* to improve convergence for proper selection of basis it is necessary to take into account that in close proximity to dielectric edge electromagnetic field behaves according to the law:

$$E \sim r^{\nu-\frac{1}{2}}, \tag{18}$$

where r is the distance to dielectric edge, $\nu = \frac{1}{2} - \frac{\arctan\sqrt{\eta^2-1}}{\pi}$,

$$\eta = \frac{s}{t - \sqrt{t^2 + 2s\left(\varepsilon_2\left(\varepsilon_1+\varepsilon_3\right)^2 + \varepsilon_1\left(\varepsilon_2+\varepsilon_3\right)^2\right)}},\ s = 2\left(\varepsilon_1(\varepsilon_2^2+\varepsilon_3^2) + \varepsilon_2(\varepsilon_1^2+\varepsilon_3^2) + \varepsilon_3(\varepsilon_1+\varepsilon_2)^2\right),$$

$$t = \varepsilon_3(\varepsilon_1-\varepsilon_2)^2.$$

To satisfy (18) the Gegenbauer polynomials $C_n^{\nu}(y)$ shall be used as a basis of the Galerkin method. As a consequence, scattered electromagnetic field is calculated from computed solution for functions $f^e(y)$ and $f^m(y)$.

Multimode scattering matrix can be computed from the equations:

$$S_{11}^{j_{e(m)}k_{e(m)}} = \sqrt{\frac{\int_0^{h+d} \mathbf{E}^-_{\perp 1 k_{e(m)}} \times \mathbf{H}^{*-}_{\perp 1 k_{e(m)}} \cdot \mathbf{e}_z dy}{\int_0^{h+d} \mathbf{E}^+_{\perp 1 j_{e(m)}} \times \mathbf{H}^{*+}_{\perp 1 j_{e(m)}} \cdot \mathbf{e}_z dy}}, \tag{19}$$

$$S_{21}^{j_{e(m)}k_{e(m)}} = \sqrt{\frac{\int_0^{h+d} \mathbf{E}^+_{\perp 2 k_{e(m)}} \times \mathbf{H}^{*+}_{\perp 2 k_{e(m)}} \cdot \mathbf{e}_z dy}{\int_0^{h+d} \mathbf{E}^+_{\perp 1 j_{e(m)}} \times \mathbf{H}^{*+}_{\perp 1 j_{e(m)}} \cdot \mathbf{e}_z dy}}, \tag{20}$$

where indices j_e and j_m define numbers of incident LM and LE modes, but indexes k_e and k_m define numbers of scattered LM and LE modes, $\mathbf{e}_z$ is the unit vector of z-axis, $\mathbf{E}^+_{\perp 1}, \mathbf{H}^+_{\perp 1}$ are transverse components of electrical and magnetic field in the domain 1 forward propagated, $\mathbf{E}^-_{\perp 1}, \mathbf{H}^-_{\perp 1}$ are transverse components of electrical and magnetic field in the domain 1 back propagated, $\mathbf{E}^+_{\perp 2}, \mathbf{H}^+_{\perp 2}$ are forward propagated transverse components of electrical and magnetic field in the domain 2.

Figure 6 demonstrates a comparison of computed components of scattering matrix by the proposed (BEM) and finite-difference time-domain (FDTD) methods for the structure

characterized by the parameters: ε_1=10, ε_2=1, ε_3=1, d/h=0.01, $\beta_x h = \pi / 6$. As it is seen, there is good agreement between proposed and FDTD methods. However computing time for BEM is much less than for FDTD method due to lower order of resulting system of linear algebraic equation.

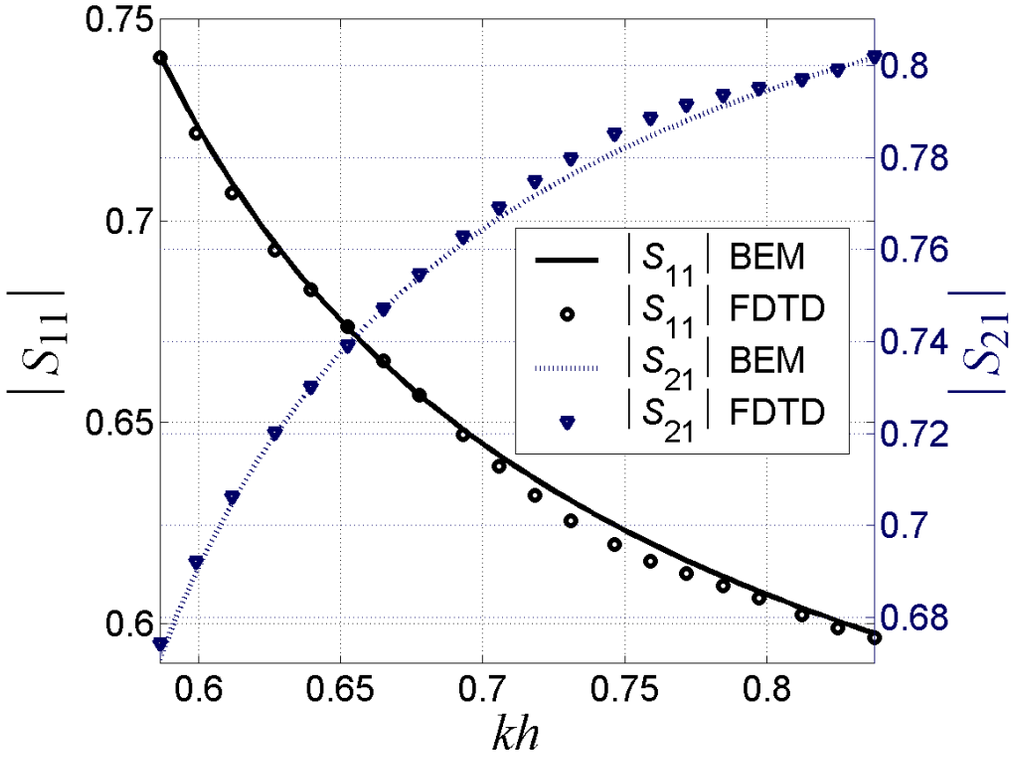

Figure 6. Reflection (S_{11}) and transmission (S_{21}) coefficients computed by boundary element (BEM) and finite-difference time-domain (FDTD) methods. ε_1=10, ε_2=1, ε_3=1, d/h=0.01, $\beta_x h = \pi / 6$

4. Effective permittivity of one-dimensional dielectric discontinuity

Transverse wavenumber defines a propagation constant of the structure presented in Figure 1, which contains a discontinuity. Effective permittivity of the structure can be stated as such permittivity of homogeneous structure, which gives numerically the same propagation constant as in inhomogeneous structure. The effective permittivity of basic LM mode can be easily recomputed from transverse wavenumber by the equation:

$$\varepsilon_{eff} = \varepsilon_1 - \frac{\beta_{y1}^{e\ 2}}{k^2} \quad . \tag{21}$$

As it follows from the equation (21), nature of the dependence of effective permittivity on distance between metal plate to dielectric is determined by the function $\beta_{y1}^{e}(d)$. Let's consider alteration limit of effective permittivity while displacement of metal plate under the dielectric. It follows from equation (21) that relative alteration of effective permittivity can be derived from the equation:

$$\delta\varepsilon_{eff} = \frac{\varepsilon_1 - \varepsilon_{eff}}{\varepsilon_1} = \frac{\tilde{\beta}_{y1}^{e\ 2}}{\varepsilon_1 \tilde{k}^2}\ , \tag{22}$$

where $\tilde{\beta}_{y1}^{e} = \beta_{y1}^{e} h$ is normalized transverse wavenumber in domain filled by dielectric with permittivity ε_1 and $\tilde{k} = kh$ is normalized propagation constant in free space.

Utmost value of the normalized transverse wavenumber is equal to $\pi/2$ (Figure 2). Therefore for large values of normalized propagation constant $\tilde{k}$ maximal alteration of normalized effective permittivity is restricted by the value $\delta\varepsilon_{eff\,\max} < \frac{\pi^2}{4\varepsilon_1 \tilde{k}^2}$. Criterion of large and small values of $\tilde{k}$ will be determined below.

As it follows from (22) relative alteration of effective permittivity is increased while normalized propagation constant is reduced. Utmost range of the alteration can be found on the assumption of $\tilde{k} \to 0$. At this assumption as it is seen from (1) normalized transverse wavenumber $\tilde{\beta}_{y1}^{e}$ tends to zero as well. In this case the equations (1) can be solved analytically:

$$\lim_{\tilde{k}\to 0} \tilde{\beta}_{y1}^{e} = \sqrt{\frac{\left(\varepsilon_1 - \varepsilon_2\right)\frac{d}{h}}{\frac{\varepsilon_2}{\varepsilon_1} + \frac{d}{h}}}\,\tilde{k}\ . \tag{23}$$

Substitution of (23) into (22) gives utmost value of relative alteration of effective permittivity:

$$\lim_{\tilde{k}\to 0} \delta\varepsilon_{eff} = \frac{\varepsilon_1 - \varepsilon_2}{\varepsilon_2 \frac{h}{d} + \varepsilon_1}\ . \tag{24}$$

It is seen that on the assumption of $\tilde{k} \to 0$ effective permittivity can be controlled from ε_1 to ε_2. If medium in domain 2 (Figure 1) is air, then the range of effective permittivity alteration due to displacement of metal plate is from ε_1 to 1. Such high controllability is not available in other methods of control including electrical bias control of ferroelectrics.

Graphically dependence (24) is presented in Figure 7. This dependence demonstrates utmost controllability of effective permittivity of the dielectric discontinuity by alteration of distance between metal plate and dielectric if medium in the domain 2 is air. For certain permittivity ε_1 the dependence is an upper asymptote for other values of $\tilde{k}$. For $\tilde{k} \neq 0$ analogous dependences stand below those presented in Figure 7.

Due to limitation of effective permittivity alteration from ε_1 to ε_2 and utmost value of normalized transverse wavenumber equal to $\pi/2$, to achieve utmost controllability the normalized propagation constant shall satisfy to requirement:

$$\tilde{k} < \frac{\pi}{2\sqrt{\varepsilon_1 - \varepsilon_2}}. \tag{25}$$

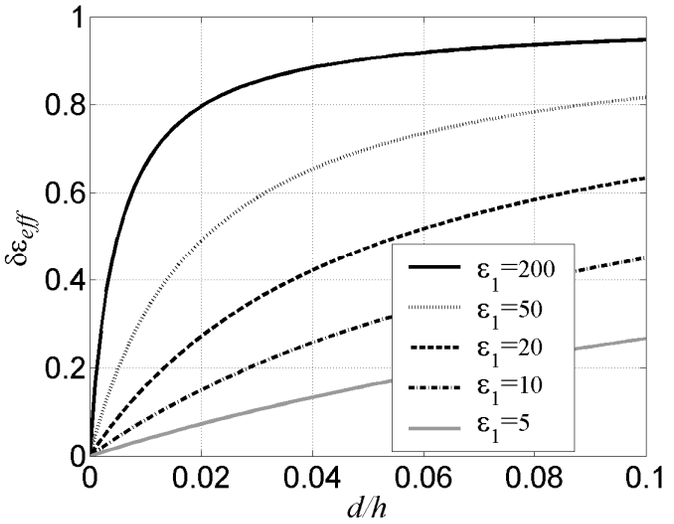

Figure 7. Dependence of relative alteration of effective permittivity on distance between metal plate and dielectric on the assumption of $\tilde{k} \to 0$.

Neglect of requirement (25) leads to decrease of controllability range and ε_{eff} is limited by the value $\varepsilon_1 - \frac{\pi^2}{4\tilde{k}^2} > \varepsilon_2$. The same conclusion can be derived from analysis of the formula (24) on the assumption of $\frac{d}{h} \to \infty$ and solution of equations (1).

Figure 8 demonstrates influence of normalized propagation constant on utmost range of effective permittivity alteration. This picture reflects dependence of relative alteration of effective permittivity on normalized distance between metal plate and dielectric with permittivity $\varepsilon_1 = 50$. For this permittivity of dielectric the requirement (25) is transformed to $\tilde{k} < \frac{\pi}{14} \approx 0.224$. As it is seen in Figure 8 if the last requirement is not satisfied then the range of effective permittivity alteration is considerably reduced and if $\tilde{k} = 0.6$ is only equal to 10% from ε_1 , and if $\frac{d}{h} > 0.02$ then effective permittivity is almost independent on distance between metal plate and dielectric. Similar phenomenon in waveguides filled by multilayer dielectric if phase velocity of electromagnetic wave is almost independent on sizes of high-permittivity dielectrics was named as dielectric effect or effect of dielectric waveguide.

As it is seen in Figure 8 dependence of alteration of effective permittivity on normalized propagation constant has opposite trend than analogous dependence of alteration of transverse wavenumber (see Figure 2, *a*): controllability of transverse wavenumber is increased while propagation constant is risen up but controllability of effective permittivity

is reduced at the same condition. The point is that the controllability of effective permittivity depends on ratio of transverse wavenumber to propagation constant rather than transverse wavenumber.

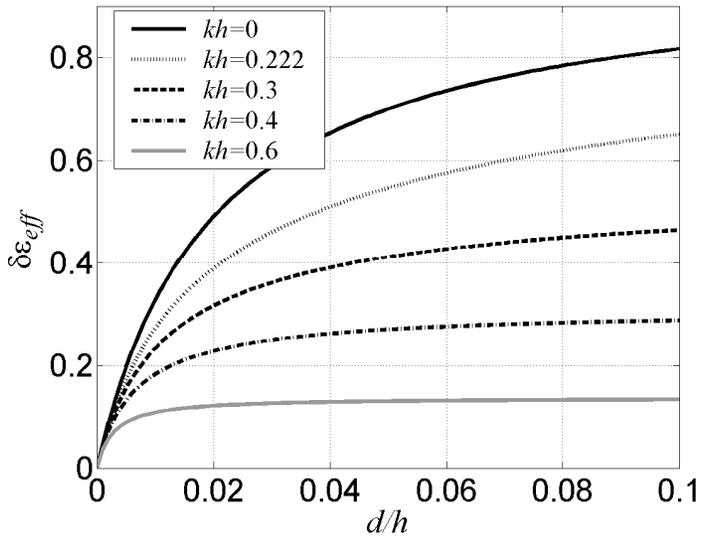

Figure 8. Dependence of relative alteration of effective permittivity on distance between metal plate and dielectric for certain normalized propagation constant kh while $\varepsilon_1 = 50$, $\varepsilon_2 = 1$.

Requirement (25) can be considered as criteria of smallness of normalized propagation constant. If this requirement is satisfied then the normalized propagation constant may be considered as small, otherwise as large.

Hereby to increase controllability of effective permittivity one should reduce normalized propagation constant. It can be done by two ways. The first method is decreasing of working frequency. However this way has limitation because for many implementations the frequency shall exceed cutoff frequency and cannot be reduced. The second way is to reduce thickness of dielectric h. It follows from (25) that efficient controllability of effective permittivity the thickness should to satisfy the requirement:

$$h < \frac{\pi}{2k\sqrt{\varepsilon_1 - \varepsilon_2}}. \tag{26}$$

If requirement (26) is not satisfied then the range of effective permittivity alteration is decreased according to the law close to $\sim h^{-2}$. Moreover required displacement of metal plates for effective permittivity control would be increased.

Effective permittivity model simplifies understanding and simulation of phenomena in controllable microwave devices. This model accurately describes wavelength of fundamental mode in controllable structure. However accuracy of scattering problem description should be investigated. Let's compare scattering matrix derived from effective permittivity model and rigorous solution of scattering problem by the BEM described above.

Scattering matrix for effective permittivity approach can be found from equations:

$$S_{11} = \frac{\beta_{z1} - \beta_{z2}}{\beta_{z1} + \beta_{z2}}, \quad S_{21} = \frac{2\sqrt{\beta_{z1}\beta_{z2}}}{\beta_{z1} + \beta_{z2}}, \tag{27}$$

where β_{z1} is the propagation constant in domain 1 (Figure 5) but β_{z2} is the propagation constant in domain 2 filed by uniform dielectric with permittivity ε_{eff}.

Comparison of two techniques is demonstrated in Figure 9. Good agreement for reasonable parameters set is observed.

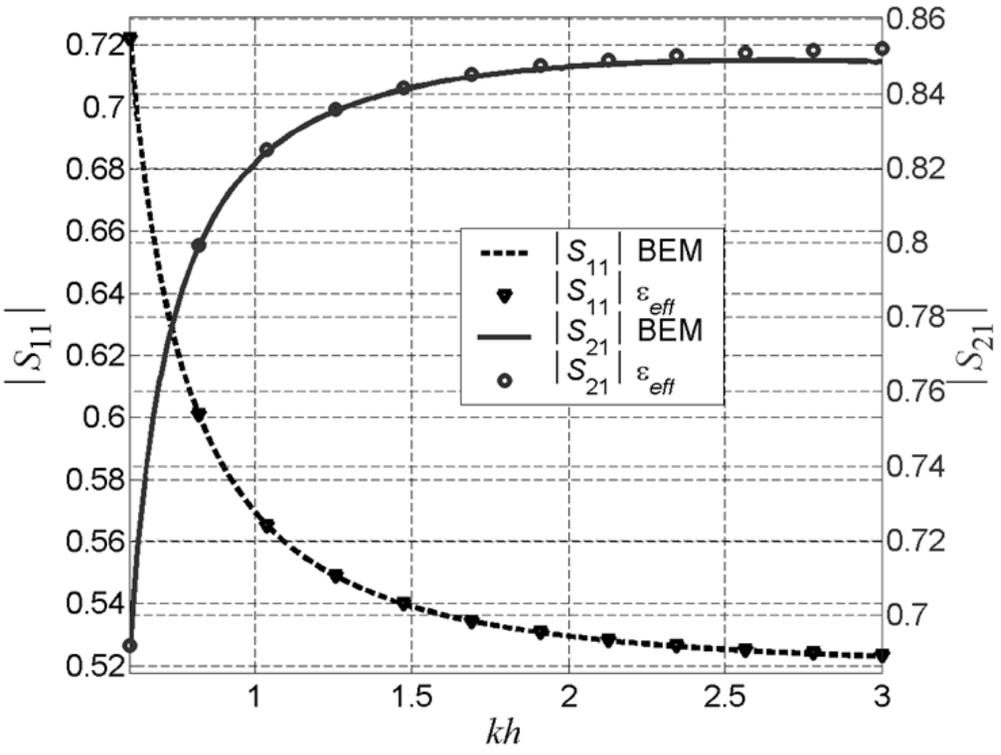

Figure 9. Comparison of *S*-parameters computation using boundary element method (BEM) and effective permittivity approach for the structure with parameters: $\varepsilon_1 = 10$, $\varepsilon_2 = 1$, $\varepsilon_3 = 1$, $d/h = 10^{-3}$

Hereby effective permittivity approach is efficient method for investigation of controllable microwave structures. Below this technique is extended for microstrip and coplanar lines.

5. Effective permittivity of microstrip and coplanar lines

Microstrip and coplanar lines are the most widely used waveguide types in modern microwave systems. They interconnect oscillators, amplifiers, antennas and so on. Sections of transmission lines also used as coupling element for resonators. Usually characteristics of the transmission line are defined at design time and remain constant in fabricated device. However, transmission lines can get some agility. For example, movement of dielectric body above microstrip or coplanar line surface results in propagation constant change [2]. We have shown that the more efficient control can be achieved, if one of the conductors is

detached from substrate's surface, Figure 10. Because controllable discontinuity crosses electric field strength lines, it results in higher sensitivity.

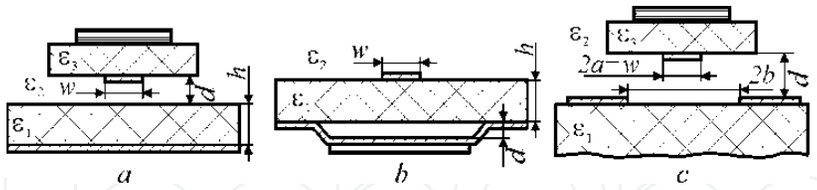

Figure 10. Mechanically controllable microstrip (*a*, *b*) and coplanar (*c*) lines

Conventional methods of microstrip lines analysis, such as Whiller equations [3], Hammerstad equations [4], and their extensions to coplanar lines [5] exploit symmetry of the line with aid of conformal mappings. These methods also introduce effective permittivity to relate quasi-TEM wave propagation characteristics to those of equivalent TEM wave. Transmission lines in Figure 10 still possess symmetry, but their rigorous analysis becomes cumbersome. Thus, numerical techniques could be applied to accurately calculate electromagnetic field distribution.

Electromagnetic problem can be solved using electric and magnetic scalar φ^e, φ^m and vector $\mathbf{A}^e$, $\mathbf{A}^m$ potentials:

$$\mathbf{E} = -i\omega\mathbf{A}^e - \nabla\varphi^e; \quad \mathbf{H} = \frac{\nabla \times \mathbf{A}^e}{\mu\mu_0}; \tag{28}$$

$$\mathbf{E} = \frac{\nabla \times \mathbf{A}^m}{\varepsilon\varepsilon_0}; \quad \mathbf{H} = -i\omega\mathbf{A}^m - \nabla\varphi^m. \tag{29}$$

Using these potentials one can introduce electromagnetic filed distribution types with one of components being zero. If electrical vector potential oriented along z axis ($\mathbf{A}^e = A^e\mathbf{e}_z$, where $\mathbf{e}_z$ is z-axis unit vector), then A^e and φ^e functions define E-type field, or TM-mode, for which $H_z = 0$. Similarly, if magnetic vector potential oriented along z axis ($\mathbf{A}^m = A^m\mathbf{e}_z$), then A^m and φ^m functions define H-type filed, or TE-mode, for which $E_z = 0$. Equation (28) is more convenient in the systems with dielectric only discontinuities, but with uniform permeability.

Equations (28), (29) allow ambiguity in relation of vector and scalar potentials with electromagnetic field components. For example, if $\mathbf{A}^e$ and φ^e define certain electromagnetic filed distribution, then $\mathbf{A}^e + \nabla\phi$ and $\varphi^e + \phi$, where ϕ is differentiable function, define the same distribution. This ambiguity is removed applying Lorentz's calibration:

$$\nabla\left(\varepsilon\nabla\varphi^e\right) + \varepsilon^2\mu\frac{\omega^2}{c^2}\varphi^e = 0. \tag{30}$$

In case of axial symmetry and absence of external currents solution of (30) may be presented in the form:

$$\varphi^e = \psi(x,y)Z(z),$$

where $\psi(x,y)$ is distribution of scalar potential in Oxy plane, $Z(z)$ is distribution along propagation direction Oz. Then (30) splits in two equations with two mentioned distribution functions. In most practical cases electric field component along direction of propagation is much smaller and could be neglected. This is so called quasi-TEM mode. Thus 3D electromagnetic problem reduces to 2D plane problem:

$$\nabla\cdot(\varepsilon\nabla\psi)+\beta^2\psi=0, \tag{31}$$

where $\varepsilon\mu\frac{\omega^2}{c^2}=\beta^2+\beta_z^2$. Applying appropriate boundary conditions the problem is solved numerically using two dimensional finite element method (2D FEM). Then one may calculate electromagnetic field distribution as:

$$E_x=-\frac{\partial\psi}{\partial x};\qquad E_y=-\frac{\partial\psi}{\partial y};\qquad E_z=-i\frac{\beta^2}{\sqrt{\varepsilon\mu\frac{\omega^2}{c^2}-\beta^2}}\psi;$$

$$H_x=Z_0^{-1}\sqrt{\frac{\varepsilon}{\mu}}\frac{\sqrt{\varepsilon\mu}\frac{\omega}{c}}{\sqrt{\varepsilon\mu\frac{\omega^2}{c^2}-\beta^2}}\frac{\partial\psi}{\partial y};\qquad H_y=-Z_0^{-1}\sqrt{\frac{\varepsilon}{\mu}}\frac{\sqrt{\varepsilon\mu}\frac{\omega}{c}}{\sqrt{\varepsilon\mu\frac{\omega^2}{c^2}-\beta^2}}\frac{\partial\psi}{\partial x},$$

where $Z_0=\sqrt{\frac{\mu_0}{\varepsilon_0}}\approx 120\pi\Omega$ is free space characteristic impedance. In most practical cases $\beta_z << \sqrt{\varepsilon\mu\frac{\omega^2}{c^2}-\beta^2}$, thus $E_z\approx 0$ and wave is close to TEM.

Having solution of (31) we introduce effective permittivity ε_{eff} relating total power in the system under consideration to power in the system with uniform filling:

$$\varepsilon_{eff}=\frac{\sum_{i=1}^{N}\left(\varepsilon_i\iint_{S_i}\left(\left(\frac{\partial\psi}{\partial x}\right)^2+\left(\frac{\partial\psi}{\partial y}\right)^2\right)dxdy\right)}{\iint_{S}\left(\left(\frac{\partial\psi_1}{\partial x}\right)^2+\left(\frac{\partial\psi_1}{\partial y}\right)^2\right)dxdy},$$

where S_i is i-th domain area with permittivity ε_i, S is line's cross section total area, ψ_1 is distribution of scalar potential in regular line with $\varepsilon_1 = 1$. Quasi-static approximation gives results, which coincide well with rigorous solution by 3D FEM and finite difference in time domain (FDTD) method (Figure 11). However, at small displacements of conductor above substrate rigorous solutions faced convergence difficulties, especially FDTD method.

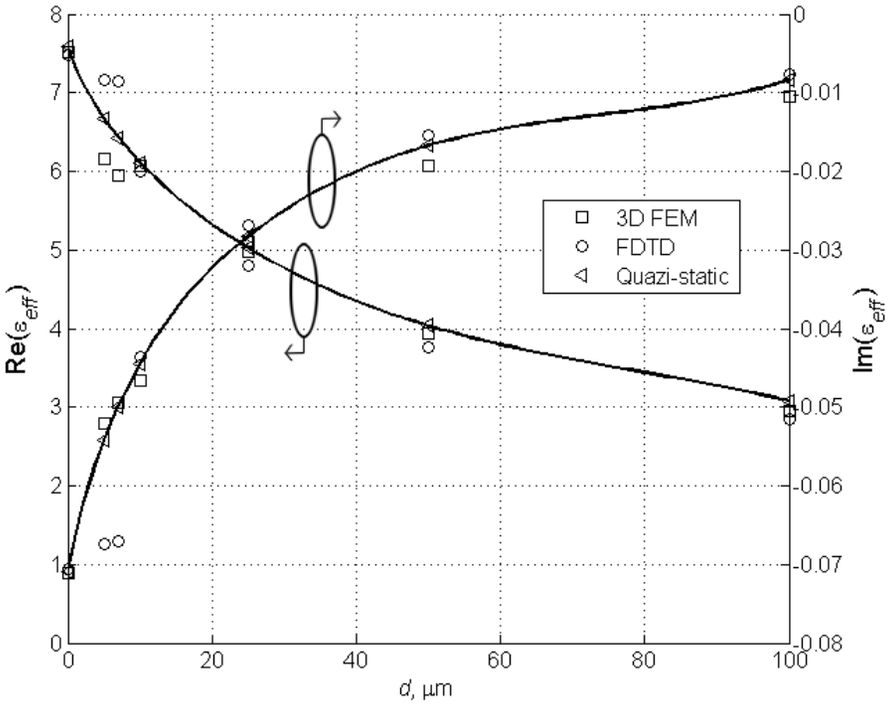

Figure 11. Comparison of effective permittivity calculation in microstrip line using 3D FEM, FDTD and quasi-static approximation ($\varepsilon_1 = 12$, $w = 0.5$ mm, $h = 1.5$ mm)

In conventional microstrip line most of electromagnetic field is confined in substrate between the strip and ground plane. When conductor is lifted above substrate as in Figure 10 *a*, *b*, certain part of electromagnetic filed redistributes from substrate to the air filled domains close to the strip. Because of lower permittivity energy stored in air filled domains is lower comparing to that one in substrate. This leads to decrease of the system's effective permittivity, as it is shown in Figure 12. Effective permittivity of the line defines wavelength in the system or, equivalently, propagation constant. Thus, mutual displacement of transmission line parts results in change of propagation constant. Described method of effective permittivity control has strong sensitivity. As seen in Figure 12 displacement by 10% of substrate's thickness may change effective permittivity more then by half.

Redistribution of electromagnetic energy to air filled domains also changes loss in the system. Because air is almost lossless medium, the portion of energy confined in air filled domains experience practically no dielectric loss. Consequently more energy reaches output terminal, resulting in lower effective loss, Figure 12.

Presented quasi-static approximation can be applied for analysis of coplanar line as well. Dependencies of effective permittivity and loss on coplanar line with lifted signal strip qualitatively similar to those of coplanar line, Figure 13.

Derived values of effective permittivity and loss then can be used to design device similarly to strict TEM-mode devices. Controllability of effective permittivity for more complicated microwave devices was presented in [1].

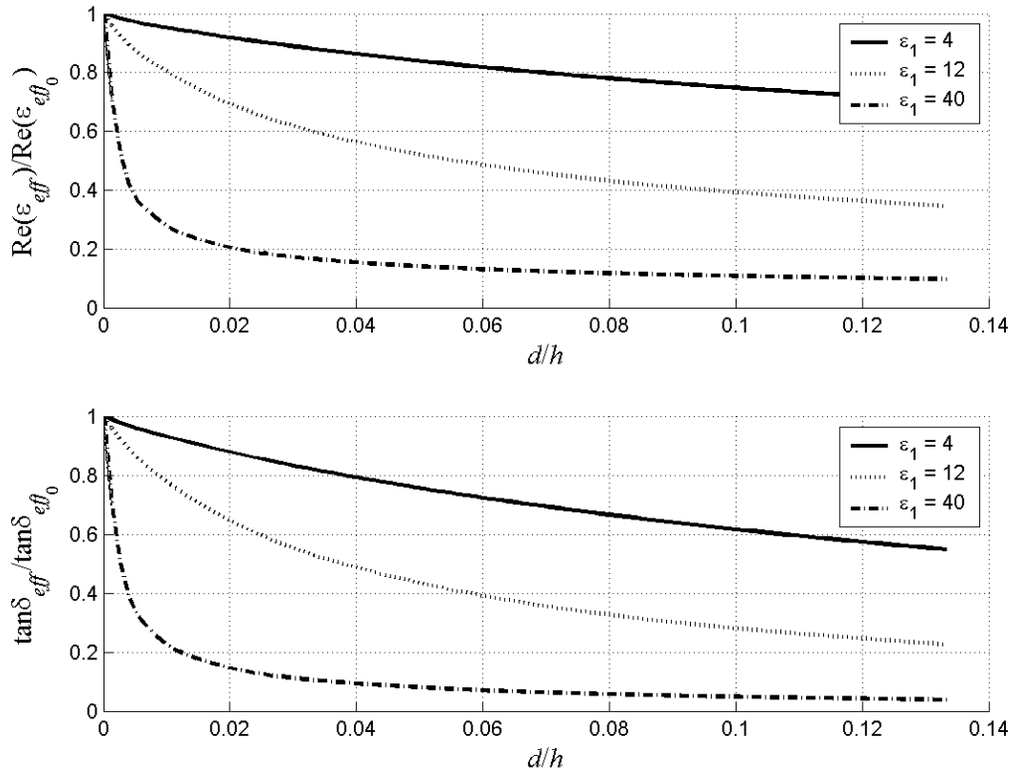

Figure 12. Effective permittivity in near 50Ω microstrip line with micromechanical control ($w/h = 2$). ε_{eff_0} and $\tan\delta_{eff_0}$ are effective permittivity and loss tangent at zero $d/h = 0$

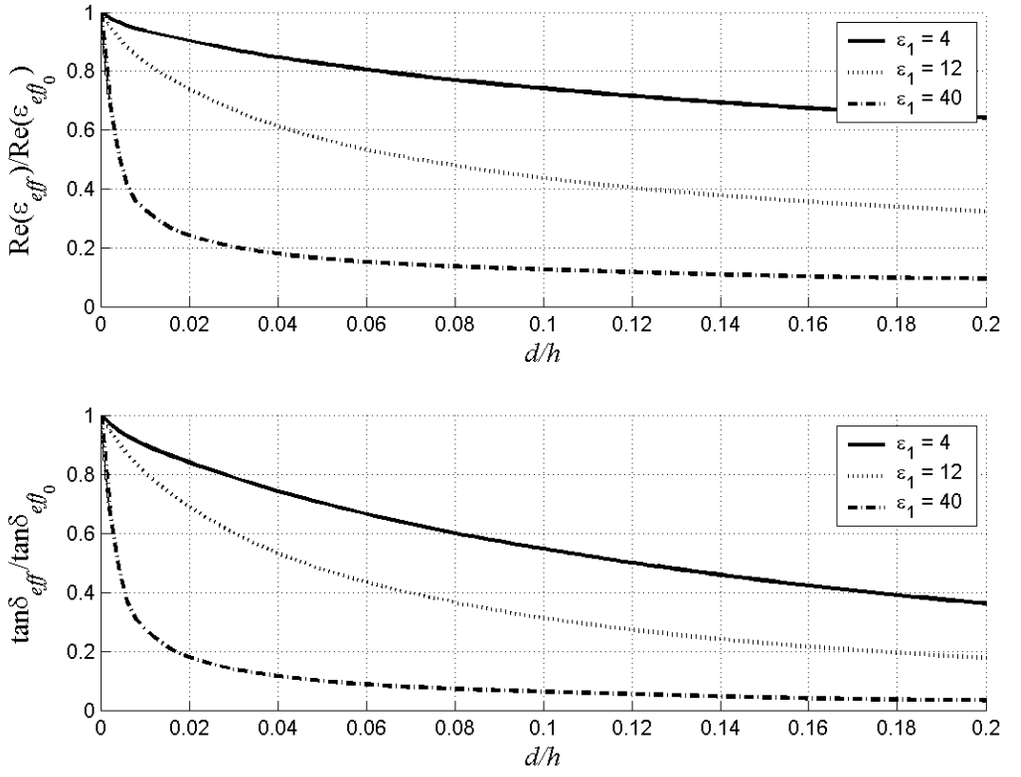

Figure 13. Effective loss in near 50Ω coplanar line with micromechanical control ($b/a = 0.72$). ε_{eff_0} and $\tan\delta_{eff_0}$ are effective permittivity and loss tangent at $d/h = 0$

Demonstrated high sensitivity of effective permittivity to microwave device parts displacement opens an opportunity to employ piezoelectric or electrostrictive actuators to control characteristics of the microwave devices by the electromechanical manner. Properties of materials for piezoelectric and electrostrictive actuators are discussed in the next section.

6. Piezoelectric and electrostrictive materials for actuators

Application of usual piezoelectric ceramics for the microwave device tuning was described previously [1, 2]. However, in a strong controlling field piezoelectric ceramics show electromechanical hysteresis that produces some inconveniences. Much more prospective are relaxor ferroelectrics that have better transforming properties and practically no hysteresis.

Ferroelectrics with partially disordered structure exhibit diffused phase transition properties. Relaxor ferroelectrics near this transition show an extraordinary softening in their dielectric and elastic properties over a wide range of temperatures. Correspondingly, dielectric permittivity ε of the relaxor shows large and broad temperature maximum where giant electrostriction is observed (because the strain x is strongly dependent on the dielectric permittivity: $x \sim \varepsilon^2$).

Relaxors are characterized by the large $\varepsilon \sim (2 - 6)\cdot 10^4$ and, consequently, by very big induced polarization P_i . A comparison of P_i in the relaxor ferroelectric $Pb(Mg_{1/3}Nb_{2/3})O_3$ = PMN and P_i of paraelectric material $Ba(Ti_{0.6},Sr_{0.4})O_3$ = BST (that also has rather big ε ~ 4000) is shown in Figure 14, *a*.

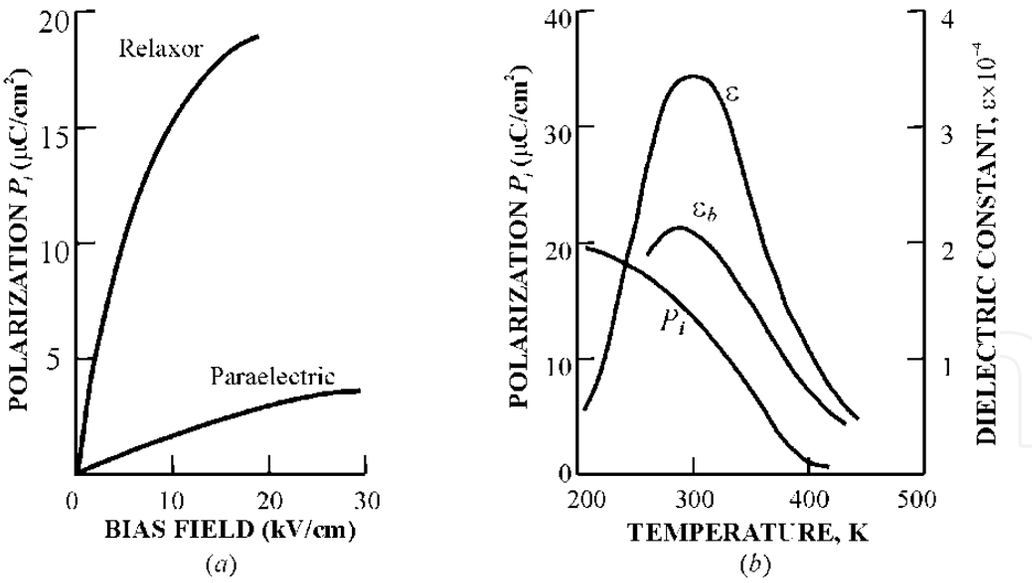

Figure 14. *a* – electrically induced polarization P_i in the relaxor of PMN and in the paraelectric BST; *b* – dielectric permittivity of PMN without (ε) and under bias field E_b=10 kV/cm (ε_b); P_i is the induced polarization in the relaxor PMN, obtained by pyroelectric measurements

Induced polarization in PMN many times exceeds one of BST. Moreover, in relaxor, the P_i depends on the temperature (like P_S of ferroelectrics), as it can be seen in Figure 14, *b*. An example is electrically induced piezoelectric effect that is explained in Figure 15.

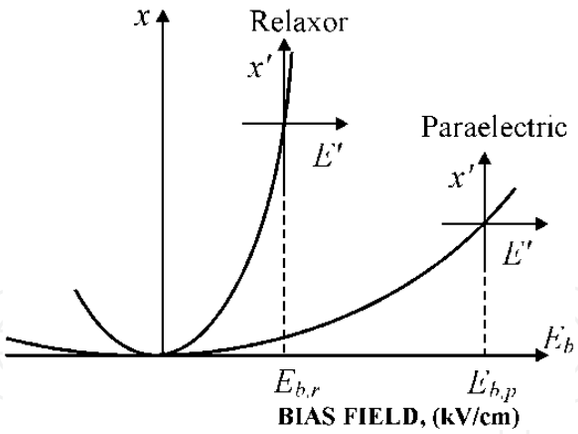

Figure 15. Electrostriction in the high-ε materials under the bias field looks like piezoelectric effect ($x' \sim E'$); $E_{b,r} < E_{b,p}$

Electric bias field E_b produces some constant internal strain x_0 at the parabolic dependency strain x on field E. Besides of steady and relatively big bias field E_b, a smaller alternating electric field E' is applied to given dielectric material. As a result, pseudo-linear "piezoelectric effect" appears that is shown in a new scale: x' - E'.

Piezoelectric effect appears instantly after the bias field is applied, and it disappears immediately after the bias field is switched off. Electrically induced piezoelectricity is large owing to giant electrostriction. Relaxor actuators can be used as precision positioner, including microwave tunable devices. Very important for device application the response time of relaxors can be estimated by the dielectric spectroscopy method.

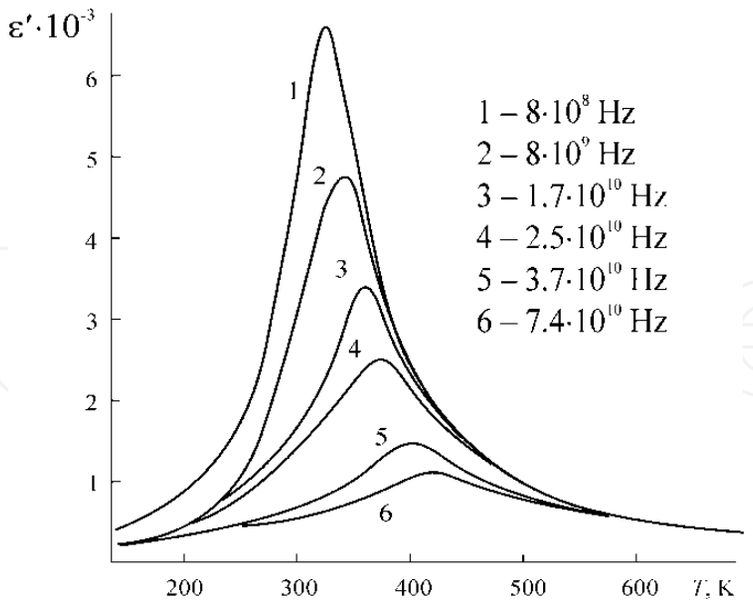

Figure 16. Dielectric spectrum of PMN at microwaves, fast dispersion of dielectric permittivity started near one gigahertz

It is obvious that response quickness is determined by the frequency dispersion of relaxor's dielectric permittivity: ε(ν). That is why dielectric dispersion in the relaxors is studied with a

point of view of relaxor material applications in the fast-acting electronic devices. By the microwave dielectric spectroscopy method conducted in a broad temperature interval, the family of $\varepsilon^*(\nu,T)=\varepsilon'(\nu,T)+i\varepsilon''(\nu,T)$ curves are obtained, and one example is shown in Figure 16.

Response time of relaxor devices is determined by the mechanisms of dielectric dispersion. Electro-mechanical contribution to relaxor ε might be dominating factor so in relaxor based electronic devices the speed of response is defined by the sound speed in the relaxor, so the operating speed is dependent on the size of used relaxor element.

7. Conclusion

To achieve electromechanical control by using piezoelectric or electrostrictive actuators the dielectric- air discontinuity should create significant perturbation of the electromagnetic field. It requires a certain location of the discontinuity relatively to electromagnetic field distribution. It was demonstrated that for maximal reconfiguration of electromagnetic field by the dielectric parts displacement the border between air slot and dielectric should be perpendicular to the electric filed. In this case the displacement of dielectric parts leads to a considerable rearrangement of the electromagnetic field, and as a result to device characteristics alteration.

Effective permittivity approach not only simplifies computation but provides information about controllability of microwave structures by alteration of air slot thickness *d* as well. The controllability depends on frequency and dielectric thickness *h*. Maximal range of effective permittivity alteration increases while either frequency or thickness *h* reduces. At the same time, the reducing of either frequency or thickness *h* leads to increase of the controllability effectiveness due to decrease of required displacement of device components. Utmost controllability of effective permittivity was obtained on the assumption that either frequency or thickness of dielectric *h* tends to zero. Calculated dependences reflect asymptotic control over effective permittivity by alteration of air slot thickness *d*. Analysis of the dependences shows that the effective permittivity may be controlled in the range from permittivity of dielectric to one. Such high controllability cannot be achieved by other methods including ferroelectric permittivity control by electrical bias.

For given working frequency effectiveness of controllability increases if thickness of dielectric layer is decreased. Criterion for maximal thickness of dielectric was estimated. It is necessary to note that decrease in dielectric thickness reduces characteristic impedance of structure. That is why adding of matching sections should be considered in actual device design.

Presented method of control not only preserves high quality factor of microwave devices in the case of application low loss dielectrics but demonstrates reducing of dielectric loss during the control as well.

Effective permittivity approach significantly simplifies simulation of microwave devices. However, this approach has limitations related with high order modes excitation. That is

why this technique should be carefully verified by the rigorous solution, boundary element method for instance.

Author details

Yuriy Prokopenko, Yuriy Poplavko, Victor Kazmirenko and Irina Golubeva
National Technical University of Ukraine "Kiev Polytechnic Institute", Kiev, Ukraine

8. References

[1] Yu. Poplavko, Yu. Prokopenko and V. Molchanov. Tunable Dielectric Microwave Devices with Electromechanical Control, Passive Microwave Components and Antennas, Vitaliy Zhurbenko (Ed.), In-Tech, 2010, p.367-382, ISBN: 978-953-307-083-4 (DOI: 10.5772/9416)

[2] T.-Y. Yun, K. Chang. A low loss time-delay phase shifter controlled by piezoelectric transducer to perturb microstrip line // IEEE Microwave Guided Wave Letters.– Mar. 2000.– Vol. 10, P. 96–98 (DOI: 10.1109/75.845709).

[3] H. A. Whiller. Transmission Line Properties of Parallel Wide Strip by Conformal Mapping Approximation // IEEE Transaction on Microwave Theory and Techniques.– 1964.– Vol. 12, P. 280–289 (DOI: 10.1109/TMTT.1964.1125810).

[4] E. Hammerstad, O. Jensen. Accurate Models for Microstrip Computer-Aided Design // IEEE MTT-S International Microwave Symposium Digest.– 1980, P. 407–409 (DOI: 10.1109/MWSYM.1980.1124303).

[5] C. Veyres, V. F. Hanna. Extension of the Application of Conformal Mapping Techniques to Coplanar Line with Finite Dimensions // International Journal of Electronics.– 1980.– Vol. 48, P. 47–56 (DOI: 10.1080/00207218008901066).